Theoretical and Experimental Second Harmonic Generation Studies of the Rotational Elastic Response of a Dye Molecule in a Random Copolymer of Styrene and Methyl Methacrylate

C. W. Dirk,* S. Devanathan, and M. Velez

Department of Chemistry, The University of Texas at El Paso, El Paso, Texas 79968-0513

F. Ghebremichael and M. G. Kuzyk

Department of Physics, Washington State University, Pullman, Washington 99164-2814

Received January 7, 1994; Revised Manuscript Received June 29, 1994®

ABSTRACT: We report on second harmonic generation measurements of a polymer-impeded electric field induced rotation of the dye molecule Disperse Red 1 in a series of styrene–methyl methacrylate copolymers of varying composition. We show, by wasy of analysis of a generalized hypothetical binomial or multinomial distribution, that the dye molecules are not randomly distributed through the polymer and apparently associate more strongly with the styrene and methyl methacrylate homopolymer regions. Alternatively, this could be viewed as evidence of nonrandom distribution of the two monomers of the copolymer. We further suggest through molecular mechanics calculations that the polymer molecular motion associated with the electric field induced rotation of the dye involves torsional rotations of the polymer side groups and main chain. It also appears that the elastic response inherent to the probe molecule constitutes no more than 10–15% of the overall elastic response measured for the probe/polymer mixture.

Introduction

Recently, Kuzyk et al. have demonstrated that molecular elastic constants of second-order nonlinear optical dye molecules in a polymer matrix can be determined by applying a static electric field and measuring the intensity of the second harmonic generated from a laser beam that passes through the sample.[1] The measurement is unique and different from the many temporal stability studies being done on poled polymer electro-optic materials in that it measures the real part of the viscoelastic response, in contrast to the many other studies[2-5] of decay which involve the slower measurement of the imaginary part. In essence, a truly elastic analysis results, which provides information about the environment around the dye molecule as well as information about the polymer itself. The only measurements of this kind have been made on pure poly(methyl methacrylate) using the dye molecule Disperse Red 1 as the probe molecule. The result for that measurement suggested that the microscopic elastic constant around the dye molecule was a factor of 10 smaller than the bulk elastic constant for the polymer. This was interpreted as suggesting weak interaction between the dye and polymer so that the elastic response of the polymer was largely disconnected from interaction of the dye molecule. In essence, the dye molecule could be viewed as rattling around in a cage with which it has a weak interaction. In order to clarify this interpretation, we have jointly undertaken the investigation of the second harmonic generation (SHG) assayed microscopic elastic response of the Disperse Red 1 dye in a series of styrene–methyl methacrylate copolymer matrices.

Before addressing the experimental results, it is important to assess the nature of the experiment being conducted. In principle, the elasticity of an object is measured by applying a force to it and measuring the resultant displacement. The elasticity can be linear, in which the force results in a translation, or torsional, in which a torque results in an angular displacement. As an example, consider a wire. If one end is fixed and a torque τ is applied to the free end, the wire will twist. If an angle of twist of the wire's end is θ, the elasticity of the wire k_θ is defined according to Hooke's law:

$$k_\theta = \tau/\theta \tag{1}$$

It is clear that the elasticity depends on both the wire's mechanical properties and its geometry.

There are thus two parameters that must be measured to determine the elasticity: the applied torque and the angle of twist. In the present work, we use a probe molecule to measure the microscopic elasticity of the polymer as follows. The dye molecules have a dipole moment μ^* so that the applied electric field, E, results in a torque

$$\tau = \mu^* E \cos\theta \tag{2}$$

where θ is the angle between the electric field and the original orientation of the molecule in the polymer. Because second harmonic generation is a sensitive measure of molecular orientation, the intensity of the second harmonic light increases when an electric field is applied to a material as the molecules reorient along the direction of the applied field. In principle, then, the applied torque to a molecule in a polymer can be determined from its dipole moment and the magnitude of the applied electric field. The degree of molecular reorientation, on the other hand, is probed by second harmonic generation. The elasticity can then be easily determined. We note that, in order for such measurements to probe the elasticity of the polymer near the molecule, the polymer must have a small second-order susceptibility and dipole moment compared with the molecule. Such is the case for the materials in the present study.

In real systems, there is a continuous distribution of orientations of dopant molecules and the second harmonic measurement probes an ensemble average. The measurement proceeds as follows. First, the second harmonic intensity, $I_{T<T_g}$, is measured in the presence of the applied electric field below the glass transition temperature where the polymer is elastic. The polymer is then heated to some temperature T above its glass transition temperature

® Abstract published in *Advance ACS Abstracts,* August 15, 1994.

0024-9297/94/2227-6167$04.50/0

where the molecules are free to reorient and the second harmonic intensity $I_{T>T_g}$ is measured for the same applied electric field. If the initial distribution is isotropic, the microscopic elasticity is of the form:

$$k_\theta = 2kT(I_{T>T_g}/I_{T<T_g})^{1/2} \quad (3)$$

where k is Boltzmann's constant. In this way, one need not know either the molecular dipole moment, μ, or the magnitude of the molecular hyperpolarizability, β. It is relevant to note that, in this procedure, the bulk second harmonic signal, $\chi^{(2)}$, is inversely related to an effective mean microscopic elastic constant, k_θ

$$\chi^{(2)} \propto 1/k_\theta \quad (4)$$

The elastic model leads to a relationship for the angle of electric field induced rotation, ϵ, of the molecule given its original angle, θ_0, with respect to the normal to the surface of the sample

$$\epsilon = \frac{(\mu^* E/k_\theta)\sin(\theta_0)}{1 + (\mu^* E/k_\theta)\cos(\theta_0)} \quad (5)$$

where μ^* is the dressed dipole moment, which accounts for the polymer polarization, E the electric field, and k_θ the microscopic elastic constant. For μE and k_θ of the magnitude of those encountered or measured here, it is relevant to note that the average electric field induced rotation is less than 1° and the maximum electric field induced rotation, ϵ (for $\theta_0 = 90°$), is on the order of 2°. Thus, the technique almost certainly does not involve significant viscous displacement of the surrounding polymer. If anything, the perturbation of the polymer involves very slight displacement, even for the rotation of a long probe molecule. The issue then arises as to whether this displacement is compressional or torsional. The magnitude of the measured elastic constant of DR1 in PMMA is 3.58×10^{-13} dyn cm. This corresponds to a value of 5.0 kcal mol^{-1} rad^{-2}. We will show that such a value is of the correct magnitude for torsional elastic rotation of the polymer around its single-bond backbone and side groups.

Thus, there are two main issues here. One is the theoretical or phenomenological explanation of the behavior of the elastic constant as a function of varying polymer composition, while the other involves interpreting the microscopic process that is occurring. An additional related issue is the rationalization of the discrepancy observed between the bulk and microscopic elastic constants. This is addressed in the context of correcting for the elasticity inherent to the probe molecule.

Experimental Section

The general procedure for preparing the styrene–methyl methacrylate random copolymers used in this work is as follows:

Monomers (obtained from Aldrich Chemical Co.) were purified by removing the inhibitor (usually a hydroquinone) by washing with 10% NaOH until the aqueous phase was colorless and then two to three times with distilled water until litmus paper was neutral and drying over Na_2SO_4. The polymerization initiator AIBN was recrystallized from methanol, collected on a glass frit, and stored in a refrigerator. The free-radical polymerization of styrene and methyl methacrylate was done by taking appropriate mole percent of the monomers (typically a total of 0.9–0.94 mol total for both monomers) in a three-necked flask, deaerating with nitrogen, affixing a water condenser, adding a solution of 200 mg of AIBN in 100 mL of benzene, and heating overnight at 60–70 °C with magnetic stirring under nitrogen. The solution was diluted with 100 mL more of benzene, and the copolymers were precipitated with the rapid addition of hexane, filtered, and then dried in a vacuum oven for 48 h. Proton NMR (Bruker, 200 MHz) analysis suggested that the polymers are random to within the error (perhaps 10–15%) of unambiguously determining the presence of the triad signals[6] resulting from the neighboring MMA and styrene (STY) monomer units. It was not possible to exclude the presence of occasional long blocks of STY or MMA using the NMR data that were available. Thus, based on NMR, there is some chance of a nonrandom distribution of monomers, perhaps up to 5–10 mol % of the polymer composition in samples in the nondilute regions (10–90 mol % STY).

Copolymer empirical compositions were determined by elemental analysis using the significant difference in carbon composition of the monomers as the basis for distinguishing their relative stoichiometry in the polymers. Given an elemental analysis uncertainty of 0.3%, this provides a mole fraction uncertainty of approximately 1 mol %.

Elastic constant measurements, sample preparation, and nonlinear optical measurements have been previously described.[1,7] Sample preparation involved spinning thin films of the copolymers on indium–tin oxide (ITO) glass (Donnelley) electrodes. The ITO plates were prepared, first by cutting into $1 \times {}^2/_3$ in. rectangles, followed by a patterning procedure to remove some of the ITO. With the long axis, platers tape ${}^1/_3$ in. wide is placed on the ITO side with ${}^1/_6$ in. clearance on either side. Several of these plates are arranged in a semiconductor wafer holder and dipped into a 10% NaOH aqueous solution for 8–10 min at 55 °C. The wafer holder is then immersed in deionized water for 5 min to remove the alkaline solution, followed by immersion in solution containing equal parts of concentrated HCl, concentrated H_2SO_4, and 8% HNO_3. A final deionized water wash is performed, the plates are allowed to dry, and the platers tape is removed. Isopropyl alcohol is used to remove tape residue. The resulting plate now has a ${}^1/_3$ in. wide ITO layer with ${}^1/_6$ in. nonconductive ITO-free strips on either side.

The copolymers were dissolved in 1,1,2-trichloroethane as 10–15% by weight solutions. The dye Disperse Red 1 was added as 10% by weight relative to the copolymer, and the solution was allowed to stir to establish homogeneity. Solutions were dropped from a syringe attached with a 25-mm 0.2-μm PTFE syringe filter (polypropylene filter housing) onto the patterned ITO plate to establish complete coverage without solution spilling off the level plate and then spun on a standard photoresist spinner for 30 s at speeds ranging from 750 to 2500 rpm to create a thin film of optimum thickness of 2–3 μm. The freshly spun ITO plate is placed on a hot plate at 100 °C for 1 min to force removal of entrained solvent.

EFISH SHG samples are created by taking two ITO plates with spun films, placing the plates face-to-face (polymer surface to polymer surface) such that the two plates are crossed perpendicularly providing a ${}^2/_3$ in. square region of overlap, and then pressed at 100 lbs force at 130 °C to establish an optical window. The polymer on the ITO which extends from the crossed section on both plates is scrapped off to permit attachment of voltage leads.

It is relevant to note that the room temperature measurements of the field-dependent second-order susceptibility were preceded by annealing the sample to temperatures 10–20 °C above the glass transition and physical aging for at least 1 week to reduce excess free volume. Samples were prepared for 25 compositions of MMA–STY copolymers. Several compositions were eliminated due to electrical shorting while applying electric fields. Several other compositions were eliminated from further study after repeated annealings could not eliminate significant zero electric field SHG. The reason for the persistent unpoled SHG in some samples is unknown and is presently under study. Polystyrene and poly(methyl methacrylate) are known to demonstrate dielectric memory or switching,[8] though the mechanism is unclear.[9,10]

Glass transition temperatures were measured on a Perkin-Elmer differential scanning calorimeter. A plot of T_g versus composition is provided in Figure 1.

PCMODEL calculations were performed with version 4.0 of PCMODEL on a DOS 33-MHz Intel 80486 based personal computer. The standard PCMODEL *mmx*[11] potential field was used for all calculations. Torsional rotational potential energy

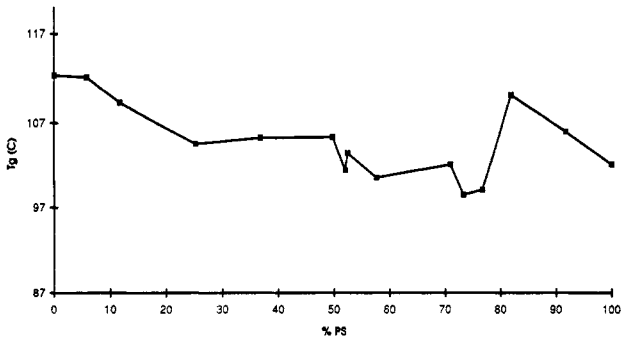

Figure 1. Plot of experimental DSC T_g versus mole fraction composition of the MMA–STY copolymers, with increasing STY concentration along the ordinate.

plots were obtained by using the dihedral driver feature of PCMODEL. This feature permits incremental rotation around a particular dihedral, followed by energy minimization following each incremental rotation. For this study, the increment for rotation was 1°. It was also decided to rotate at least 540° around the chosen dihedral angle in order to give the chosen polymer segment the opportunity to fully relax. For the structures studied here, such calculations typically required 3–36 h.

Torsional *mmx* based elastic constants k_{mmx} were determined by fitting a quadratic equation

$$E_{tor} = k'\theta^2 + q\theta + q' \tag{6}$$

to a selected region around the energy minima in the dihedral scan plots, where θ is the angle in radians, and E_{tor} is the torsional energy. Note that the rotational potential energy determined in the nonlinear optical determination of the experimental elastic constant, k_{exp}, is defined as:

$$U = \frac{1}{2}k_{exp}\theta^2 \tag{7}$$

Thus, the comparable theoretical value is $k_{mmx} = 2k'$.

Typically, regions were chosen with the criteria of excluding nonquadratic aberrations that appear as one rotates further and further from the minimum. Typically, this would include no more than a 10–20° excursion on either side of the minimum. Fitting to ranges involving small excursions from the minimum is justified, since, in this system, the molecule is never induced to rotate any more than 2°. Some of the potentials are unsymmetrical, regardless of how close to the minimum one confines the fit (*vide infra*).

Theory

For a material with more than one kind of pinning site for the dye molecule, the bulk microscopic elastic response is given by

$$k_\theta \propto \frac{1}{\sum_\xi \chi_\xi^{(2)}} = \frac{1}{\bar{X}} \tag{8}$$

where the index ξ labels the distinct sites. Each of the individual contributing $\chi_\xi^{(2)}$ are given by

$$\chi_\xi^{(2)} \propto 1/k_\xi \tag{9}$$

where k_ξ represents the elastic constant of that site. The important issue concerns the number of different kinds of sites and the distribution across sites.

The simplest approach to the distribution problem is to assume that sites are fully randomly populated. If we do this, then the problem reverts to considering how many different types of pinning points there are for a probe molecule. The smallest number of pinning points is two, since, if the molecule is being rotated around the center of mass, it must be restrained on either side by at least two pinning points. There is most likely a maximum number of pinning points which would be restricted by the maximum number of molecular contacts that can fit around the probe molecule. In the most naive interpretation of this model, a copolymer of two monomers could be represented as possessing two different kinds of pinning points, one associated with each monomer. Under these circumstances, and presuming only two pinning points per probe molecule, eq 8 can be inverted with the help of eq 9 to get the distribution $\bar{X}$, which yields a binomial distribution in composition:

$$\bar{X} = \frac{x^2}{2k_1} + \frac{2xy}{k_1 + k_2} + \frac{y^2}{2k_2} \tag{10}$$

where x represents the mole fraction of MMA and y represents the mole fraction of STY. In the approximation of small probe molecule concentration, $y = 1 - x$, and

$$\bar{X} = \frac{x^2}{2k_1} + \frac{2x(1-x)}{k_1 + k_2} + \frac{(1-x)^2}{2k_2} \tag{11}$$

Considering the effect of dye at concentration, c, one would have a trinomial distribution of $(x + y + c)^2$

$$\bar{X} = \frac{x^2}{2k_1} + \frac{2x(1-x)}{k_1 + k_2} + \frac{(1-x)^2}{2k_2} + \frac{xc}{k_1 + k_c} + \frac{c(1-x)}{k_2 + k_c} + \frac{c^2}{2k_c} \tag{12}$$

where $x + y + c = 1$, and k_c is the elastic constant represented by the probe molecule pinned by another probe molecule.

In this study, we have dealt with dye concentrations of 5% or 10% by weight, which corresponds to approximate mole fractions of 0.016 and 0.034, respectively. For the above binomial distributions, and under the restriction that k_c does not differ greatly from k_1 or k_2, one can easily calculate that the effect on $\bar{X}$ is no more than a few percent for such low concentrations.

It is important to recognize that the above distribution models embody at least two levels of naiveté. The first is that we have assumed there are only two kinds of pinning points, each associated with either monomer unit, and the second that there are a total of two pinning points. In reality, the dye is probably resting in sites where it is pinned by a varying number of polymer contacts, of varying types with different elastic responses. This yields a multinomial distribution of the type

$$(x_1 + x_2 + \ldots + x_s + c)^n \tag{13}$$

where each of the contact points of mole fraction x_i has associated with it an elastic constant of k_i. The minimum number of pinning points is two ($n = 2$), while the maximum number is dictated by the size of the probe molecule, and the limit of the van der Waals packing of polymer monomer units around the probe molecule (probably no more than n = 8–20, for a molecule the size of DR1). There is likely a peaked distribution across n, as well as a peaked distribution across k_i.

It must be recognized that, in this form, the distribution assumes complete random distribution of monomers and probe molecules. To the extent that there is nonrandom character, each term in the distribution $\bar{X}$ must be weighted by a population factor a_{np} ($0 \le a_{np} \le 1$), where n represents the order (the number of contact points) of

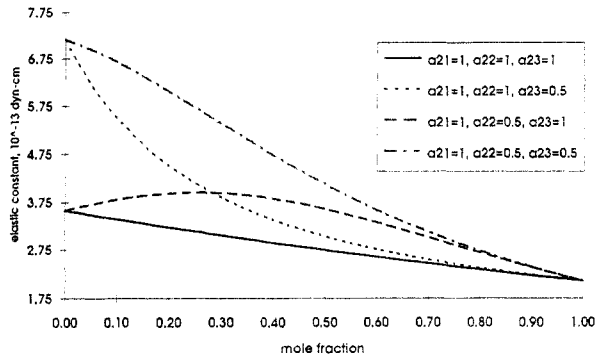

Figure 2. Plot of hypothetical binomial distribution $n = 2$ (eq 14) illustrating the effect of varying the probability coefficients $a_{n\rho}$.

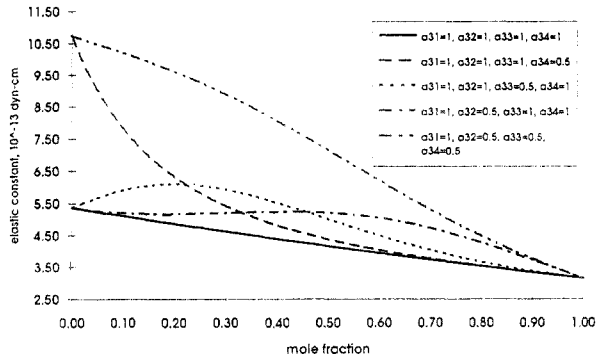

Figure 3. Plot of hypothetical binomial distribution $n = 3$, illustrating the effect of varying the probability coefficients $a_{n\rho}$.

the nomial expansion, and ρ labels the individual nomial terms in a given expansion. For example

$$\bar{X} = \frac{a_{21}x^2}{2k_1} + \frac{a_{22}2x(1-x)}{k_1 + k_2} + \frac{a_{23}(1-x)^2}{2k_2} \tag{14}$$

In a random distribution, it is important to recognize that two fundamental relationships exist:

$$\sum_{n,\rho} a_{n\rho} = 1 \tag{15}$$

and that the sum of the binomial coefficients must equal 2^n. This is true for each subdistribution defined by the integer n as long as that subdistribution is random. Regardless of the distribution, random or not, all population weighting coefficients sum to unity. A nonrandom distribution will be reflected in the shape of the distribution of k_θ versus mole fraction composition of monomer. For example, if we plot eq 14 and its related $n = 3$ higher order binomial and examine their behavior as a function of varying a_{21}, a_{22}, and a_{23} ($n = 2$; Figure 2) or a_{31}, a_{32}, a_{33}, and a_{34} ($n = 3$; Figure 3), we can see what effect should be expected. It is apparent that depending on which sites are populated (defined by the nomial term), the number of contact points (defined by n) of each, and their site frequency ($a_{n\rho}$), a plot of k_θ versus mole fraction composition could display significant structure.

It is unlikely that there are more than 20 contact points per probe molecule and that there is likely a peaked average. It may normally be unnecessary to consider nomials of n greater than 8–12. This intuitive result is important. It means that the total distribution probably encompasses at worse a sum of multinomials up to $n \approx$ 8–12. It is likely that a high percentage of the distribution will be confined to consideration of two to four multinomials, again perhaps peaked across a relatively narrow range of n. This implies that regardless of the variety of different kinds of contact points (k_is), a plot of k_θ versus mole fraction composition for a copolymer should be well represented by a polynomial of order 10–12 or less.

The complexity enters when one considers that there may be many different kinds of pinning points (each with different k_is). There is a likelihood that a significant portion of the total number of pinning points is represented by less than 20 types of pinning points. This is hard to justify explicitly. However, if one examines the MMA repeat unit, for instance, a space-filling model yields no more than 11 contact points. These are not independent of one another, so that some pinning points are essentially equivalent to others. The three hydrogens of the methyl ester are, for instance, equivalent, because they involve the same torsional potential. The total number of partially independent van der Waals contacts for the MMA unit is 5, though they may not necessarily represent significantly different k_i. Again, some naiveté is assumed here since we assume that the k_i of one pinning point is not necessarily affected by the contact with a pinning point of a neighboring polymer chain, other than to contribute as a spring in series or in parallel. The theory of elastic springs enters here where the elastic constant of springs in series is given by

$$\frac{1}{k} = \frac{1}{k_\alpha} + \frac{1}{k_\beta} + \frac{1}{k_\gamma} + \ldots \tag{16}$$

and the elastic constant of springs in parallel is given by

$$k = k_\alpha + k_\beta + k_\gamma + \ldots \tag{17}$$

so that the pinning elastic constant for a pinning point is actually best represented by an effective elastic constant for that point, which is itself better defined by the combination of springs in series and parallel.

A consequence of this argument is that the elastic constant of an infinite number of springs in series is zero. This is a catastrophe that can be averted by the consideration of the never absent background thermal motion which either adds or subtracts from the elastic effect measured at one point. While we do not treat this subject physically here, it is assumed that the background thermal motion results in regions of the polymer being effectively vibrationally isolated from other regions on some scale short of macroscopic. Another view not invoking waves or thermodynamics involves considering the polymer to possess "pinning" or chain entanglement[12-14] sites where the word "pinning" in quotations is used to represent defects where polymer chains may be tangled to create springs-in-parallel connecting regions of springs-in-series. A possible consequence of either of these mechanisms is that local pinning points may possess effective k_is that may be dominated by the local torsional rotational potential energy defining the pinning point but that all pinning points may be averaged a bit by the longer range connection to springs in parallel or series.

Results

The elastic constant (k_{exp}) inferred from the measurement of $\chi^{(2)}$ above the glass transition and at room temperature is plotted versus composition in Figure 4. Note that the plot is peaked near the center, suggesting as defined above either that the probe dye (DR1) is not randomly distributed or possibly that the polymer itself is significantly nonrandom. Nonrandom behavior of the polymer can occur due to a nonrandom chain distribution. Nonrandom behavior can also occur in a polymer that is

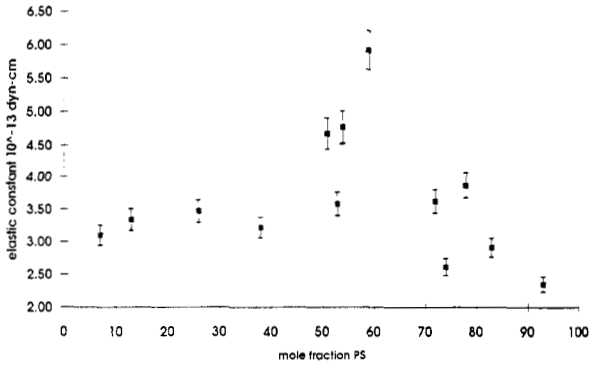

Figure 4. Plot of experimental microscopic elastic constants versus mole fraction PS.

chain-random by aggregation of monomer units from different chains, especially if stimulated by the presence of a solute such as the probe molecule. To some extent, this is equivalent to a nonrandom dye distribution. It is relevant to note that Mikhailov et al. observed a loss tan-(δ) profile versus PS–PMMA composition very similar to the optical result observed here, demonstrating a peak approximately in the same mole fraction region and of the same approximate magnitude.[15,16] It is possible that the peak in that dielectric-composition distribution is related to the same nonrandom copolymer distribution inferred here.

With the limited number of compositions, it is impossible to contemplate anything more than a fit to an approximation of the statistical distribution outlined above. We choose here to consider simple models involving no more than two microscopic spring types, k_M and k_S to correspond to the monomers MMA and STY, respectively. We also limit consideration to one binomial distribution, n, at a time.

For each of the binomial distributions, n, there are polynomials which correspond to the multinomials. For instance, we fit the data for $n = 2$

$$\frac{1}{k_{exp}} = \frac{a_{21}x^2}{2k_S} + \frac{a_{22}2x(1-x)}{k_S + k_M} + \frac{a_{23}(1-x)^2}{2k_M} \tag{18}$$

to the polynomial

$$\frac{1}{k_{exp}} = A_2x^2 + B_2x + C_2 \tag{19}$$

where the binomial weighting factors are given by

$$a_{21} = 2k_S(A_2 + B_2 + 3C_2) \tag{20}$$

$$a_{22} = k_S\left(\frac{m+1}{2}\right)(B_2 + 2C_2) \tag{21}$$

$$a_{23} = 2mk_SC_2 \tag{22}$$

$$k_S = 1/\left(2A_2 + \left(\frac{m+5}{2}\right)B_2 + (3m+7)C_2\right) \tag{23}$$

We have also chosen the binomials $n = 3$,

$$\frac{1}{k_{exp}} = \frac{a_{31}x^3}{3k_S} + \frac{a_{32}3x^2(1-x)}{2k_S + k_M} + \frac{a_{33}3x(1-x)^2}{k_S + 2k_M} + \frac{a_{34}(1-x)^3}{3k_M} \tag{24}$$

$$\frac{1}{k_{exp}} = A_3x^3 + B_3x^2 + C_3x + D_3 \tag{25}$$

$$a_{31} = 3k_S(A_3 - B_3 - C_3 - D_3) \tag{26}$$

$$a_{32} = (m+2)k_S\left(B_3\omega vr_3 + \frac{2C_3}{3} + D_3\right) \tag{27}$$

$$a_{33} = (1+2m)k_S\left(\frac{C_3}{3} + D_3\right) \tag{28}$$

$$a_{34} = 3mk_SD_3 \tag{29}$$

$$k_S = 1/\left(3A_3 + \left(\frac{m-7}{3}\right)B_3 + \frac{4(m-1)}{3}C_3 + 6mD_3\right) \tag{30}$$

$n = 4$,

$$\frac{1}{k_{exp}} = \frac{a_{41}x^4}{4k_S} + \frac{a_{42}4x^3(1-x)}{3k_S + k_M} + \frac{a_{43}6x^2(1-x)^2}{2k_S + 2k_M} + \frac{a_{44}4x(1-x)^3}{k_S + 3k_M} + \frac{a_{45}(1-x)^4}{4k_M} \tag{31}$$

$$\frac{1}{k_{exp}} = A_4x^4 + B_4x^3 + C_4x^2 + D_4x + E_4 \tag{32}$$

$$a_{41} = 4k_S(A_4 + B_4 + C_4 + D_4 + E_4) \tag{33}$$

$$a_{42} = k_S\left(\frac{m+3}{4}\right)(B_4 + 2C_4 + 3D_4 + 4E_4) \tag{34}$$

$$a_{43} = k_S\left(\frac{m+1}{3}\right)(C_4 + 3D_4 + 6E_4) \tag{35}$$

$$a_{44} = k_S\left(\frac{1+3m}{4}\right)(D_4 + 4E_4) \tag{36}$$

$$a_{45} = 4k_SmE_4 \tag{37}$$

$$k_S = 1/\left(4A_4 + \left(\frac{19+m}{4}\right)B_4 + \left(\frac{70+10m}{12}\right)C_4 + \left(\frac{15+5m}{2}\right)D_4 + (10+10m)E_4\right) \tag{38}$$

and $n = 5$,

$$\frac{1}{k_{exp}} = \frac{a_{51}x^5}{5k_S} + \frac{a_{52}5x^4(1-x)}{4k_S + k_M} + \frac{a_{53}10x^3(1-x)^2}{3k_S + 2k_M} + \frac{a_{54}10x^2(1-x)^3}{2k_S + 3k_M} + \frac{a_{55}5x(1-x)^4}{k_S + 4k_M} + \frac{a_{56}(1-x)^5}{5k_M} \tag{39}$$

$$\frac{1}{k_{exp}} = A_5x^5 + B_5x^4 + C_5x^3 + D_5x^2 + E_5x + F_5 \tag{40}$$

$$a_{51} = 5k_S(A_5 + B_5 + C_5 + D_5 + E_5 + F_5) \tag{41}$$

$$a_{52} = k_S\left(\frac{4+m}{5}\right)(B_5 + 2C_5 + 3D_5 + 4E_5 + 5F_5) \tag{42}$$

$$a_{53} = k_S\left(\frac{3+2m}{10}\right)(C_5 + 3D_5 + 6E_5 + 10F_5) \tag{43}$$

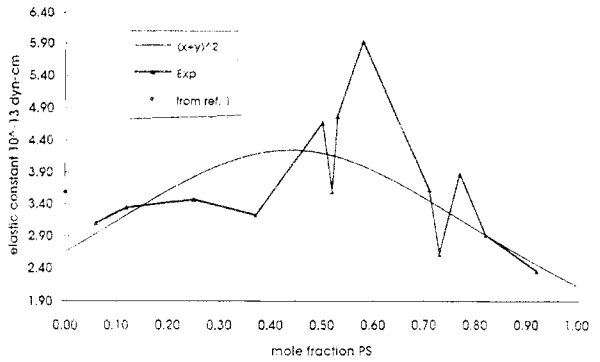

Figure 5. Fit of $n = 2$ binomial (eq 18) to experimental data. The point for 100% MMA has been included on this plot from the earlier study,[1] but not included in the nomial fit.

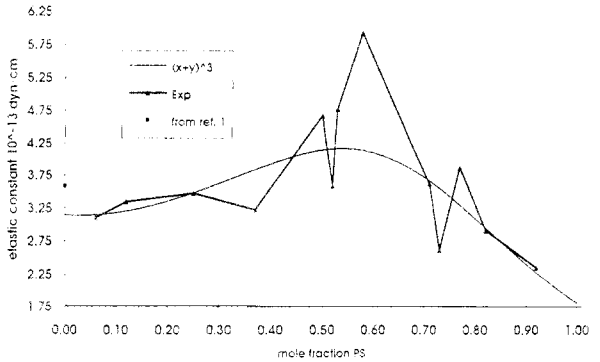

Figure 6. Fit of $n = 3$ binomial (eq 24) to experimental data. The point for 100% MMA has been included on this plot from the earlier study,[1] but not included in the nomial fit.

$$a_{54} = k_S\left(\frac{2+3m}{10}\right)(D_5 + 4E_5 + 10F_5) \quad (44)$$

$$a_{55} = k_S\left(\frac{1+4m}{5}\right)(E_5 + 5F_5) \quad (45)$$

$$a_{56} = 5k_S m F_5 \quad (46)$$

$$k_S = 1/\left(5A_5 + \left(\frac{29+m}{5}\right)B_5 + \left(\frac{69+6m}{10}\right)C_5 + \left(\frac{85+15m}{10}\right)D_5 + (11+4m)E_5 + (15+15m)F_5\right) \quad (47)$$

representing sites where there are three, four, and five pinning points, respectively. Fitting to higher order binomials ($n > 6$) is possible, though is systematically less meaningful given the number of data points. Such a fit would involve at least 8 independent parameters to fit only 13 data points which themselves are known only to 10%. The ambiguity of the five pinning point fit ($n = 5$) suggests (*vide infra*) that fitting to even higher order binomials is nonproductive at the level of approximation being tested here and given the amount of data available.

The quantity m is a parameter representing the ratio of MMA k_M pinning constant to the k_S pinning constant: $k_M = mk_S$. We have included this adjustable parameter in order to investigate the behavior of the fit under all possible combinations of k_S and k_M. By examining Figures 5–8, it is obvious that none of the fits correlate the data any more than very approximately, though one fit, $n = 4$, seems to rationalize the previously determined experimental value for neat PMMA, which is included in the figures but was excluded from the fits.

It should be recognized that all of the binomial representations of the polynomial fits are extreme approximations in that we are excluding the possibility of

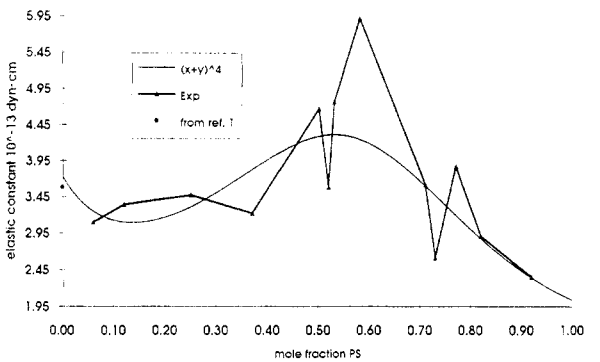

Figure 7. Fit of $n = 4$ binomial (eq 31) to experimental data. The point for 100% MMA has been included on this plot from the earlier study,[1] but not included in the nomial fit.

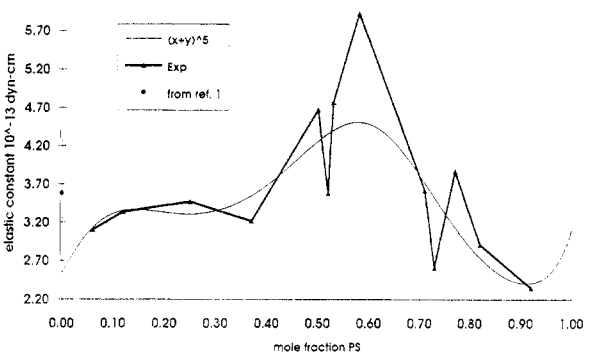

Figure 8. Fit of $n = 5$ binomial (eq 39) to experimental data. The point for 100% MMA has been included on this plot from the earlier study,[1] but not included in the nomial fit.

Table 1. Fitted Binomial Results for Selected Values of m^a

		$m = 1$	$m = 0$	$m = \infty$
$n = 2$	k_S	0.302 (0.434)	0.400 (0.576)	0
	k_M	0.302 (0.434)	0	1.238 (1.782)
	a_{21}	0.739	0.978	0
	a_{22}	0.033	0.022	0.067
	a_{23}	0.228	0	0.933
$n = 3$	k_S	0.132 (0.190)	0.168 (0.242)	0
	k_M	0.132 (0.190)	0	0.608 (0.875)
	a_{31}	0.735	0.938	0
	a_{32}	0.006	0.005	0.009
	a_{33}	0.134	0.057	0.411
	a_{34}	0.126	0	0.580
$n = 4$	k_S	0.164 (0.236)	0.304 (0.437)	0
	k_M	0.164 (0.236)	0	0.359 (0.516)
	a_{41}	0.322	0.595	0
	a_{42}	0.201	0.279	0.110
	a_{43}	−0.026	−0.024	−0.029
	a_{44}	0.327	0.151	0.535
	a_{45}	0.176	0	0.384
$n = 5$	k_S	0.110 (0.158)	0.212 (0.305)	0
	k_M	0.110 (0.158)	0	0.231 (0.332)
	a_{51}	0.179	0.341	0
	a_{52}	0.448	0.690	0.188
	a_{53}	−0.377	−0.439	−0.319
	a_{54}	0.526	0.406	0.664
	a_{55}	0.007	0.002	0.010
	a_{56}	0.217	0	0.457

[a] Note that k_M and k_S are in units of 10^{-13} dyn cm, or in parentheses are in units of kcal mol^{-1} rad^{-2}. The constants a_{np} are unitless.

the simultaneous occurrence of pinning sites with different n. As such, the missing pinning terms, $a_{ph}p!x^{p+1-h}(1-x)^{h-1}/((p+1-h)!(h-1)!)$ (for binomials of order $p \neq n$), are embedded in the few a_{nl} that are determined for a given fit n. It is likely that the large negative coefficient for the a_{53} term for the $n = 5$ fit is a result of missing binomial terms of lower or higher order. Consequently, we need to be cautious in the interpretation of the plots presented in Figures 5–8. One possible assessment based

Table 2. Elastic Constants for Trimer Units[a]

s#	MMA-(MMA)-MMA elastic constant, kcal mol^{-1} rad^{-2}	s#	MMA-(MMA)-STY elastic constant, kcal mol^{-1} rad^{-2}	s#	STY-(MMA)-STY elastic constant, kcal mol^{-1} rad^{-2}
			Axis α		
s1	5.40[0.15]⟨0.03⟩{4}	s3	5.60[0.04]⟨0.03⟩{4}	s6	5.52[0.09]⟨0.03⟩{4}
s2	6.30[0.14]⟨0.03⟩{4}	s4	4.54[0.03]⟨0.02⟩{4}	s7	3.69[0.02]⟨0.02⟩{4}
		s5	5.56[0.02]⟨0.03⟩{4}		
			Axis β		
s2	6.564⟨0.008⟩; 21.68⟨0.02⟩	s3	20.778[0.008]⟨0.026⟩{2}; 6.56⟨0.01⟩	s6	18.44⟨0.08⟩; 6.44⟨0.04⟩
		s4	24.15⟨0.03⟩; 6.92⟨0.01⟩	s7	26.14⟨0.06⟩; 8.03⟨0.04⟩
		s5	21.48⟨0.05⟩; 8.924⟨0.008⟩		
			Axis γ		
s1	19.37⟨0.02⟩; 17.07⟨0.03⟩	s3	13.37⟨0.07⟩; 12.07⟨0.08⟩; 12.9⟨0.1⟩	s6	8.48⟨0.08⟩; 5.74⟨0.08⟩
s2	16.78⟨0.01⟩; 24.40⟨0.01⟩	s4	15.71⟨0.05⟩; 23.32⟨0.06⟩	s7	14.48⟨0.02⟩; 16.32⟨0.04⟩
		s5	12.32⟨0.03⟩; 13.07⟨0.1⟩		
			Axis δ		
s1	18.12[0.72]⟨0.18⟩{4}	s3	16.94[0.82]⟨0.09⟩{4}	s6	12.27[0.48]⟨0.10⟩{4}
s2	17.29[0.96]⟨0.21⟩{4}	s4	15.07[0.65]⟨0.20⟩{4}	s7	16.82[0.09]⟨0.07⟩{4}
		s5	12.19[0.43]⟨0.16⟩{4}		

[a] The elastic constant pertains to the monomer unit in parentheses and the corresponding axis of rotation. Data are reported for data originating from different optimized starting structures s#. Data are reported in the format: average elastic constant[standard deviation of average]⟨sum of the quadratic function fit standard deviations (eq 6)⟩{number of individual values averaged}.

Table 3. Elastic Constants for Trimer Units[a]

	ϵ, MMA-(STY)-MMA
s8	5.12⟨0.02⟩; 5.68⟨0.04⟩
s9	6.338⟨0.009⟩; 6.464⟨0.008⟩
	ϵ, MMA-(STY)-STY
s10	7.54⟨0.02⟩; 5.11⟨0.03⟩; 4.82⟨0.03⟩
s11	3.338⟨0.008⟩; 3.41⟨0.03⟩
s12	4.880⟨0.004⟩; 5.092⟨0.009⟩
	ϵ, STY-(STY)-STY
s13	4.59⟨0.02⟩; 3.28⟨0.02⟩
s14	6.28⟨0.02⟩; 5.83⟨0.02⟩
	φ, MMA-MMA-MMA
s15	15.86⟨0.02⟩; 24.87⟨0.04⟩; 16.34⟨0.04⟩; 24.88⟨0.04⟩; 14.86⟨0.04⟩; 13.11⟨0.05⟩
s16	19.070⟨0.008⟩; 16.72⟨0.03⟩; 18.44⟨0.04⟩; 26.84⟨0.06⟩; 24.04⟨0.04⟩; 12.93⟨0.05⟩
	ζ, STY-STY-STY
s17	15.74⟨0.01⟩; 15.32⟨0.05⟩; 10.25⟨0.08⟩; 16.38⟨0.08⟩

[a] The elastic constant pertains to the monomer unit in parentheses and the corresponding axis of rotation. The phenyl (axis ϵ) and backbone axis (φ and ζ) elastic constants are as defined in the text. Data are reported for data originating from different optimized starting structures s#. Data are reported in the format: elastic constant⟨standard deviation of the quadratic function fit to eq 6⟩. All elastic constants are in units of kcal mol^{-1} rad^{-2}.

upon the figures is that the probe molecule is not as likely to be found pinned both by STY and MMA units as it is to be found pinned solely by STY or MMA units. This conclusion is drawn from the consideration that the middle binomial terms all contain at least one term that is close to zero for all values of m (Table 1). Another consideration is that the dye molecule is randomly distributed, but the copolymer itself is not random, implying that there are isolated regions of PMMA and PS. One cannot exclude the possibility that both the dye and monomer distributions are simultaneously nonrandom.

PCMODEL *mmx* Based Elastic Constants. Elastic constants calculated from PCMODEL are given in Tables 2–4. In order to check for systematic variation due to slightly different starting structures, in some cases we concluded several studies of the same torsional feature, though starting from slightly different initially optimized structures. These slightly different starting structures are indicated by s1, s2, s3, ..., etc. Each was the result of a separate PCMODEL *mmx* optimization. The side-group

Table 4. Elastic Torsional Constants of Disperse Red 1, As Determined from PCMODEL Results[a]

rotation axis	elastic constant, kcal mol^{-1} rad^{-2}
κ_1	51.2[0.7]⟨0.02⟩{2}
κ_2	67.9[2.1]⟨0.1⟩{3}
κ_3	64.6[3.0]⟨0.5⟩{3}
κ_4	10.09[0.60]⟨0.05⟩{5}
	20.0[1.5]⟨0.1⟩{3}[b]

[a] Data are reported in the format: average elastic constant[standard deviation of average]⟨sum of the quadratic function fit (eq 6) standard deviations⟩{number of the individual quadratic fit values averaged}. Elastic constants were based solely on the *mmx* potential unless otherwise indicated. [b] Based on PCMODEL calculation using *mmx* potential with UHF SCF π-electron calculation.

torsional features we examined were as illustrated:

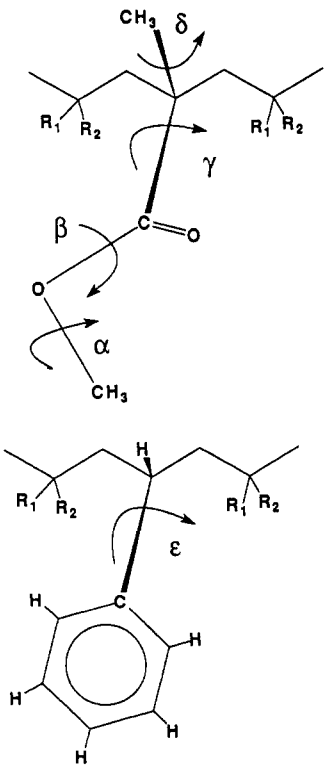

In order to simulate more effectively the role of neighboring monomer units, we examined trimers of the

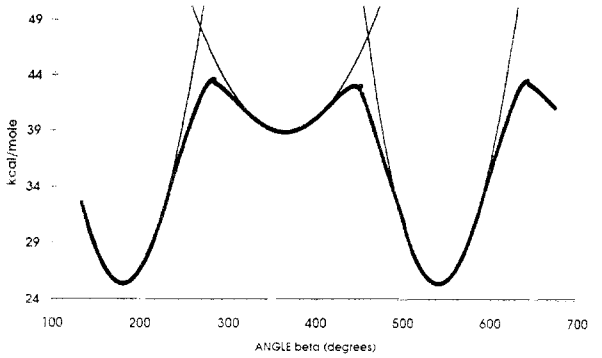

Figure 9. Plot of a dihedral scan around axis β with *mmx* minimization at each point (filled circles ●). The quadratic curves (solid lines) are the result of fitting eq 6 to each energy well.

type MMA–(MMA)–MMA, MMA–(MMA)–STY, STY–(MMA)–(STY), STY–(STY)–MMA, MMA–(STY)–MMA, and STY–(STY)–STY, where the monomer unit in parentheses was the unit under study. When it was obvious that the typical 540° rotations resulted in multiple identical energy wells, as, for instance, would be expected when rotating a methyl group, we averaged the results of those rotations for a given study s#. Otherwise, individual elastic constants for all energy wells determined by way of a dihedral scan are supplied. In the case of backbone torsions, we conducted the following studies

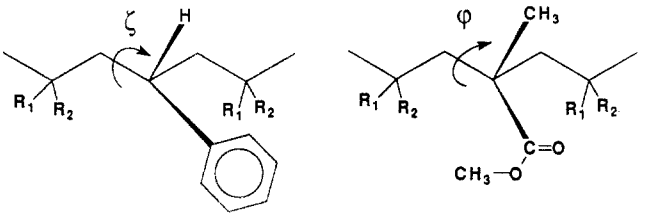

for the oligomers MMA–MMA–MMA and STY–STY–STY.

We also investigated the rotational elastic response in the DR1 molecule,

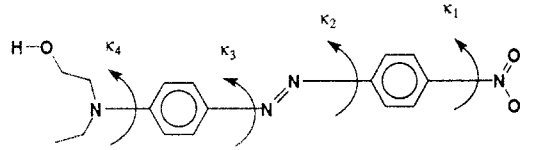

in order to ascertain to what extent the probe molecule is contributing to the news it reports about the surrounding polymer. This involved determining the *mmx* based elastic constants for rotation around four key torsional wells, defined as κ_1, κ_2, κ_3, and κ_4.

Rotations of the methyl ester methyl group (axis α) should be independent of oligomer type, since this group is remote from all other interactions in the trimer. However, one can see that the elastic constant ranges fairly broadly from 3.69 to 6.30 kcal mol^{-1} rad^{-2}. Thus, one should expect some systematic variation across data sets from varying starting structures s# in all calculated elastic constants presented here. Rotation around axis β results in two clearly distinct energy wells (Figure 9), one that varied from 6.44 to 8.92 kcal mol^{-1} rad^{-2} and another considerably steeper well with a variation of 18.44–26.14 kcal mol^{-1} rad^{-2}. Rotation around axis γ resulted in a very wide variation from 5.74 to 24.40 kcal mol^{-1} rad^{-2}. There should be two different wells, one corresponding to the gauche conformation of the ester carbonyl between the backbone segments,

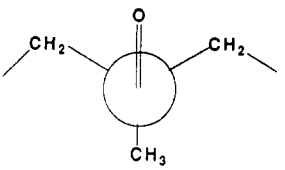

and the other a gauche conformation of the carbonyl ester between a backbone chain and the MMA α-methyl group.

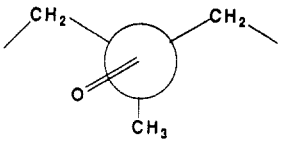

Presumably, the energy well is steeper on one side than the other. There is a potential problem with this since we fit a symmetric quadratic which might be expected to yield an average value. In some cases, based on the quality of the data, we chose an unsymmetrical fit, with more points on one side of the well than the other. This would bias the quadratic fit toward either the more or less steep side. Thus, it is likely the lowest values (<10 kcal mol^{-1} rad^{-2}) represent the elastic response for the less steep side, while the highest values (19–25 kcal mol^{-1} rad^{-2}) are more representative of the elastic response of the steeper side. Intermediate values are likely an artifact of the inadvertent averaging effect of the quadratic fit.

Rotation around the δ axis should be symmetric. Even so, a wide variation is observed between 12.27 and 18.12 kcal mol^{-1} rad^{-2}. For all fits, around all axes α, β, γ, and δ, there is no obvious systematic variation across the three possible trimers, suggesting that adjoining side groups separated by a methylene along the main chain have relatively little noticeable affect on this elastic constant. Elastic constants for rotation around the ϵ axis varied from 3.28 to 7.54 kcal mol^{-1} rad^{-2}. Again, there is no obviously apparent systematic variation across the three possible trimers. By examining Newman projections,

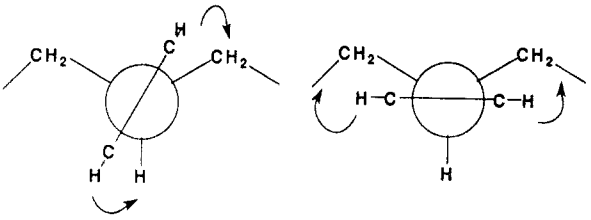

an asymmetry in at least one potential well is to be expected. Thus, it is likely that the low and high values are characteristic of the two different well edges, while the intermediate values may be more reflective of the quadratic fit averaging the well asymmetry.

Rotation around the axis φ

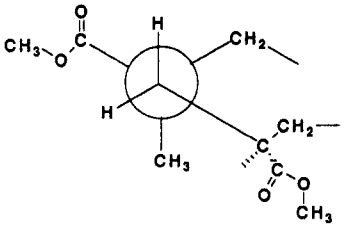

will be subject to the effects of potential energy well asymmetry, since all wells will result in unsymmetrical

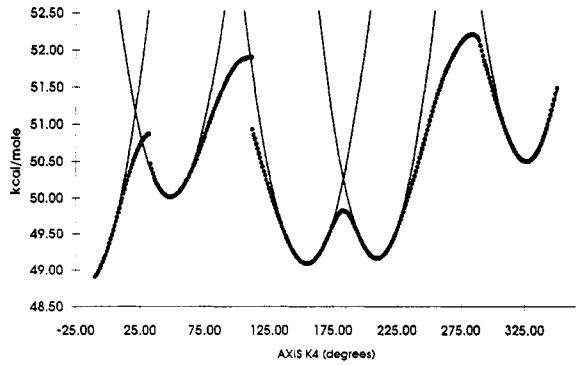

Figure 10. Plot of a dihedral scan around axis κ_4 of the molecule DR1 with *mmx* minimization at each point (filled circles ●). The quadratic curves (solid lines) are the result of fitting eq 3 to each energy well.

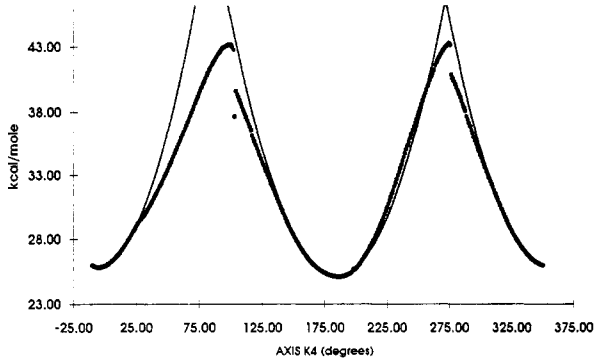

Figure 11. Plot of a dihedral scan around axis κ_4 of the molecule DR1 with *mmx* minimization including UHF SCF π-electron calculation at each point (filled circles ●). The quadratic curves (solid lines) are the result of fitting eq 3 to each energy well.

torsional interactions. The consequence of this is that there could be six different elastic constants, depending on which gauche conformation exists and which direction the rotation takes. Torsional elastic responses determined (the s15 and s16 studies) for the φ axis rotation ranged from 12.93 to 26.84 kcal mol^{-1} rad^{-2}, with an average value of 19.00 kcal mol^{-1} rad^{-2}. Rotation around the ζ axis also results in unsymmetrical torsional interactions. Torsional elastic responses ranged from 10.25 to 16.28 kcal mol^{-1} rad^{-2}, averaging 14.4 kcal mol^{-1} rad^{-2}.

The elastic constants for rotation within the probe molecule DR1 are quite large, with the exception of the *mmx*-only determination around the phenylaniline nitrogen bond, κ_4, which is comparable to other elastic responses calculated for groups in the polymer. The large elastic responses κ_1, κ_2, and κ_3 can easily be rationalized in terms of the effect of π-electron conjugation between the amine and the nitro group. This electron delocalization obviously will make rotation of the "single" bonds energetically unfavorable with regard to rotation about nonconjugated single bonds. If anything, the axis κ_4 displays a smaller than expected elastic response for an amine through-conjugated to a nitro group. It is possible the *mmx* potential is underestimating the effect of the nitrogen lone pair overlap with the phenyl ring. In order to clarify this, we conducted a dihedral drive scan with the *mmx* potential and also including a simultaneous UHF SCF π-electron calculation included in the PCMODEL program. This calculation gave a much cleaner dihedral scan (Figure 10) than did the *mmx*-only calculation (Figure 11), supplying obvious minima when the amino group became coplanar with the benzene ring. The elastic response derived from this calculation is twice that from the *mmx*-only calculation and is more in keeping with other DR1 torsional elastic constants.

Based on all of the DR1 elastic constants, as a whole, it appears that the DR1 molecule can be considered a relatively rigid rotor compared to the surrounding polymer. If a correction were made for the probe molecule contributions to the measured elastic constant, it would normally be considered as an in-series sum of the probe molecule elastic constants

$$k_{DR1} = \left(\frac{1}{\kappa_1} + \frac{1}{\kappa_2} + \frac{1}{\kappa_3} + \frac{1}{\kappa_4}\right)^{-1} \tag{48}$$

in series with the pinning sites with the polymer, effectively increasing the observed elastic constant, k_S or k_M, by

$$(k'_S)^{-1} \approx (k_S)^{-1} - \frac{1}{n}(k_{DR1})^{-1} \quad \text{or} \quad (k'_M)^{-1} \approx (k_M)^{-1} - \frac{1}{n}(k_{DR1})^{-1} \tag{49}$$

where k'_S and k'_M are approximately corrected for the effect of the DR1 torsion. The DR1 elastic constant is weighted by $1/n$ to correct for the strain of the probe being distributed among the n pinning sites. While the probe molecule is not an idle spectator, its unusual inflexibility relative to the polymer implies that its contribution is relatively small, accounting for no more than 10–15% of the elastic response, as an upper limit. This might not be the case when measuring a considerably stiffer polymer, so that stiffer probes will need to be designed for further measurements.

For the purposes of further argument, we apply a simple average of the *mmx* data for each of the rotation axes across the set of trimers, unless obviously distinctly different wells were resolvable (for instance, the β axis). This results in the following PCMODEL based elastic constants: k_α = 5.2 kcal mol^{-1} rad^{-2}, $k_{\beta 1}$ = 7.2 kcal mol^{-1} rad^{-2}, and $k_{\beta 2}$ = 22.1 kcal mol^{-1} rad^{-2} for the two clearly distinct energy wells; k_γ = 16.2 kcal mol^{-1} rad^{-2}, k_δ = 15.5 kcal mol^{-1} rad^{-2}, k_ϵ = 5.2 kcal mol^{-1} rad^{-2}, k_φ = 19.0 kcal mol^{-1} rad^{-2}, k_ζ = 14.4 kcal mol^{-1} rad^{-2}.

Using these values, we can calculate elastic constants for combinations of these functionalities in series or in parallel. For instance, using the rule for springs in series, the elastic constant for the MMA ester, k_{est}, is 2.5 kcal mol^{-1} rad^{-2} (using $k_{\beta 1}$) or 3.3 kcal mol^{-1} rad^{-2} (using $k_{\beta 2}$), when pressing against the ester methyl group. Depending on the binomial fit (n), the experimental k_M elastic constant ranges as high as 1.8 kcal mol^{-1} rad^{-2} (n = 2). This is the same order of magnitude of that predicted from the simple *mmx* based analysis for k_{est}. That the experimental value is less than that predicted based solely on the ester functionality possibly suggests that some of the strain induced in the ester is transferred to backbone as well as possibly neighboring groups. Ignoring side group and interchain interactions, and using the rules of adding springs in series and parallel, one can calculate that the strain induced in an MMA ester is transferred up to six C–C bond units in either direction away from the initially strained MMA unit, for the binomial case of n = 2 (three C–C bond units if using k'_M). The corresponding value for a strained STY unit (k_S = 0.576, n = 2) is 44 C–C bond units (36 C–C bond units when using k'_S), suggesting that styrene oligomeric segments should be much less stiff than MMA oligomeric segments. Such calculations are crude, especially when ignoring the effect of other side groups and interchain interactions, but probably supply an order of magnitude indication of the extent of torsional deformation induced by the probe molecule. These estimates,

corresponding to the upper limits for k_S ($m = 0$) and k_M ($m = \infty$), respectively, are based on a model incorporating the side group spring constant, k_{est} or k_ϵ, in series with a series of backbone spring constants, k_φ or k_ζ;

$$(k_M)^{-1} = (k_{est})^{-1} + (2\sigma k_\varphi)^{-1} \quad \text{or} \quad (k_S)^{-1} = (k_\epsilon)^{-1} + (2\sigma k_\zeta)^{-1} \quad (50)$$

where σ is the extension of the strain, in main chain C–C bond units, in either direction away from the initially strained monomer unit.

The real utility of these crude calculations is to show that the difference between the experimentally derived k_S or k_M and the calculated torsional elastic responses can be rationalized in terms of a network of springs in series or parallel. One can then also estimate that a deformation at one microscopic point of the polymer must be damped either by standing waves or elastic cross-linking sites (springs in parallel), so that another probe molecule more than six repeat units distant will probably not notice the field-dependent motion of its neighbor probe molecule, at least given the polymer impedance at room temperature. Schaefer's NMR results[17] suggest a short-range collective four-carbon main-chain motion for PMMA, in qualitative agreement with the elastic response range inferred here. Ignoring side group and interchain interactions in the estimate of σ means that σ is determined as an upper limit. Inclusion of such interactions would likely lead to a closer coincidence with the motion inferred by NMR. Similar magic angle spinning NMR results by Schaefer on PS were less conclusive but do not eliminate the possibility of longer range elastic responses for PS oligomeric units.

Conclusions

It appears that the NOMEC (nonlinear optical measurement of elastic constant) technique developed by Kuzyk et al. supplies information regarding the torsional elastic response environment of the polymer surrounding the probe molecule. In particular, the calculated molecular elasticity agrees well with the measured value considering the crudeness of the model. Furthermore, the prediction of a six C–C unit motion is reasonably consistent with NMR results. It is significant to note that the probe molecule apparently contributes little to the measured elastic response (no more than 10–15%) due to its stiffness. Now that we have constructed a model that is consistent with the measured microscopic elasticities, we plan to study the observed order of magnitude difference between the bulk elastic response and the microscopic elastic response, which may be due to some unknown collective interaction on a scale larger than the probe molecule.

Acknowledgment. We gratefully acknowledge support from a UTEP University Research Initiative Grant, The Texas Advanced Research Program & Texas Higher Education Coordinating Board (Grant No. 003661-012), and the donors of the Petroleum Research Fund.

References and Notes

(1) Kuzyk, M. G.; Moore, R. C.; King, L. A. *J. Opt. Soc. Am. B* **1990**, *7*, 64.
(2) Kohler, W.; Robello, D. R.; Dao, P. T.; Willand, C. S.; Williams, D. J. *J. Chem. Phys.* **1990**, *93*, 9157.
(3) Boyd, G. T.; Francis, C. V.; Trend, J. E.; Ender, D. A. *J. Opt. Soc. Am. B* **1991**, *8*, 887.
(4) Hampsch, H. L.; Yang, J.; Wong, G. K.; Torkelson, J. M. *Polym. Commun.* **1989**, *30*, 40.
(5) Hampsch, H. L.; Yang, J.; Wong, G. K.; Torkelson, J. M. *Macromolecules* **1990**, *23*, 3648.
(6) Slonin, I. Y.; Lyubimov, A. N. *The NMR of Polymers*; Plenum Press: New York, 1970.
(7) Kuzyk, M. G.; Singr, K. D.; Zahn, H. E.; King, L. A. *J. Opt. Soc. Am. B* **1989**, *6*, 742.
(8) Sakai, Y.; Sadoka, Y.; Okada, G. *J. Mater. Sci.* **1984**, *19*, 1333–1338.
(9) Sadoka, Y.; Sakai, Y. *J. Chem. Soc., Faraday Trans. 2* **1976**, *72*, 1911.
(10) Henisch, H. K.; Meyers, J. A. *Thin Solid Films* **1978**, *51*, 265.
(11) Gajewski, J. J.; Gilbert, K. E.; McKelvey, J. *Adv. Mol. Model.* **1990**, *2*, 65–92.
(12) Kausch, H. H.; Dettenmaier, M. *Colloid Polym. Sci.* **1982**, *260*, 120–123.
(13) Muller, F. H. *Kolloid Z.* **1941**, *95*, 138.
(14) Muller, F. H. *Kolloid Z.* **1941**, *95*, 306.
(15) Michailow, G. P. *Makromol. Chem.* **1960**, *35*, 26–53.
(16) Borosova, T. I.; Mikhailov, G. P. *Vysokomol. Soedin.* **1959**, *1*, 563–573.
(17) Schaefer, J.; Stejskal, E. O.; Buchdahl, R. *Macromolecules* **1977**, *10*, 384–404.